

Characteristics of solar diurnal variations: a case study based on records from the ground magnetic observatory at Vassouras, Brazil

Klausner V.^{a,b}, Papa A. R. R.^{a,c}, Mendes O. Jr.^b, Domingues M. O.^d, Frick P.^e

^aNational Observatory - ON 20921-400, RJ, Brazil

^bDGE/CEA/National Institute for Space Research - INPE 12227-010 São José dos Campos, SP, Brazil

^cRio de Janeiro State University - UERJ, RJ, Brazil

^dLAC/CTE/National Institute for Space Research - INPE 12227-010 São José dos Campos, SP, Brazil

^eInstitute of Continuous Media Mechanics, Perm, Russia

Abstract

The horizontal component amplitudes observed by ground-based observatories of the INTER-MAGNET network have been used to analyze the global pattern variance of the solar diurnal variations. Data from magnetic stations present gaps in records and consequently we explored them via a time-frequency gapped wavelet algorithm. After computing the gapped wavelet transform, we performed wavelet cross-correlation analysis which was useful to isolate the period of the spectral components of the geomagnetic field in each of the selected magnetic stations and to correlate them as function of scale (period) with the low latitude Vassouras Observatory, Rio de Janeiro, Brazil, which is under the South Atlantic Magnetic Anomaly (SAMA) influence and should be used as a reference for an under-construction Brazilian network of magnetic observatories. The results show that the records in magnetic stations have a latitudinal dependence affected by the season of year and by the level of solar activity. We have found a disparity on the latitudinal response at southern and northern hemispheres during solstice, which is expected due to the asymmetry of the Sq field. On the other hand, records from magnetic stations located at approximately the same latitude but at different longitudes presented peculiar dissimilarities. These results suggest that quiet day patterns and the physical processes involved in their formation still remain an important issue, far from being fully understood.

Keywords: Magnetogram data, H component, Quiet days, Gapped Wavelet analysis, Wavelet Cross-correlation.

1. Introduction

The daily variations of the geomagnetic field were discovered by the english researchers Graham and Watchmaker (1724) through the observation of a compass needle motions in 1722. Since then, it is well known that a typical spectrum of those magnetic variations is composed by a few harmonics of the 24-h period (12, 8 and 6-h). They are described as “quiet daily geomagnetic field variations” - referred to as “Sq” for “solar quiet” field Campbell (1989).

The traditional method of calculating the baseline for the quiet day variations is to use the five quietest day for each month for each magnetic observatory. In this work, we propose a new way to deal with quiet periods by eliminating the disturbed days using a multiscale process. To accomplish this task, we study the harmonics of the solar diurnal variations using hourly data of

11 the H component and explore it via a gapped wavelet technique (described in Frick et al., 1997).
12 The gapped wavelet technique is suitable for analysis of data with gaps. In our case, datasets,
13 from various magnetic stations that present gaps in the records in different periods of time (see
14 Frick et al. (1998) for mathematical motivation and proofs) were analyzed.

15 Originally wavelet transforms were applied in geophysics to analyze seismic signals in the
16 pioneer works of Morlet (1983) and Grossmann and Morlet (1984). Nowadays, the use of the
17 wavelet technique has exponentially grown in many different areas. A similar trend is noted in
18 the application of the wavelet cross-correlation technique, which has been used by many work-
19 ers. It was first introduced by Nesme-Ribes et al. (1995) to study two time series of solar data.
20 Frick et al. (2001), in space research, analyzed optical and radio maps of the nearby spiral galaxy
21 NGC 6946 using the correlation between images as function of scale.

22 Nevertheless, the wavelet cross-correlation can be used for many other different approaches
23 and purposes. For instance, Oczeretko et al. (2006) used the wavelet cross-correlation method to
24 assess the synchronization between contractions in different topographic regions of the uterus,
25 as a potential diagnostic alternative in several pathologies. More recently, Rehman and Siddiqi
26 (2009) researched correlations between pairs of time series of meteorological parameters such as
27 pressure, temperature, rainfall, relative humidity and wind speed to study the climatic dynamics
28 at different locations.

29 This work aims mainly to highlight and interpret the solar diurnal variations at a Brazilian
30 station compared to other twelve magnetic stations reasonably well distributed over the whole
31 Earth's surface. By applying gapped wavelet transforms to these signals, we were able to ana-
32 lyze both the frequency content of each signal and the time dependence of that content. After
33 computing the wavelet transform, we performed wavelet cross-correlation analysis, which was
34 useful to isolate the period of geomagnetic spectral components in each station and to correlate
35 them as function of scale (period).

36 The rest of the paper is organized as follows: Section 2 is devoted to explain the principal
37 mechanisms and aspects of the solar magnetic variations. In Section 3, the analyzed period and
38 data are presented. Section 4 describes, divided in subsections, the used methodology: Sec-
39 tion 4.1 presents a brief description of continuous wavelet transforms, Section 4.2 is devoted to
40 introduce the gapped wavelet analysis, and Section 4.3 to establish the wavelet cross-correlations
41 and to explain how they can be quantified. In Section 5, the results are discussed and, finally,
42 Section 6 brings the conclusions of this work.

43 2. The Physics of the Solar Magnetic Variation

44 The major driving force for quiet day field changes seems to arise from the dynamo-current
45 process in the ionospheric E region between 90 and 130 km (Stewart, 1882). Tidal winds move
46 the ions across the Earth's magnetic field producing electro-magnetic forces (emfs). Those emfs
47 drive electric currents in the conducting E region which give rise to daily variations in the mag-
48 netic field measured at the ground level (for details see Chapman and Bartels, 1940). Through
49 these mechanisms, two vortices of currents are induced, one in the northern hemisphere (clock-
50 wise) and another in the southern hemisphere (counterclockwise). At the same time, a strong
51 eastward electric jet is formed throughout the equatorial region.

52 There are three factors that affect the dynamo process: the ionospheric wind, the ionospheric
53 conductivity and the geomagnetic field configuration. The wind and the conductivity vary sea-
54 sonally due to their dependence on the solar zenith angle (Campbell, 1989). Zhao et al. (2008)

concluded that the correlation between the Sq amplitude and solar zenith was better in high latitude than in low latitude regions due to the effect of the prenoon-postnoon asymmetry of Sq.

The Sq field variation has a main spatial dependence on latitude and is affected by other factors including epoch of the year and level of solar activity. Chapman and Stagg (1929) observed two kinds of regular changes in the solar diurnal magnetic variations on quiet days: annual variation, that affects both the type and the amplitude during each year; and solar activity variation, that affects fundamentally the amplitude along each sunspot cycle. Takeda (1999) estimated that the intensity of the Sq currents in high solar activity was about twice larger than in low solar activity.

Many other researchers studied the variations of the Sq, including Hibberd (1985) that examined the annual, semi-annual and even the whole solar cycle. Stening (1971) examined seasonal variations and longitudinal inequalities of the electrostatic-field in the ionosphere by looking at its electric conductivity and the Earth's main magnetic field. Takeda (2002) showed solar activity dependence of the Sq amplitude, and explained this effect through the ionospheric conductivity. Takeda (2002) also compared the amplitude of the Sq for the same value of conductivity. The seasonal variation is seemingly due to differences in neutral winds or to the magnetic effect of the field-aligned current (FAC) flowing between the two hemispheres generated by the asymmetry in the dynamo action. The FACs are controlled by interplanetary magnetic fields (IMF) and its electric fields can directly penetrate to the equatorial ionosphere (Sastri, 1988).

Some evidence of the influence of oceanic tides on the magnetic daily variation has been obtained by Larsen and Cox (1966). They found small semidiurnal variations of the Z component at a coastal site (Cambria, California) and at two island stations (Honolulu and San Miguel) that could not be explained by the atmospheric tidal theory. They suggested that these variations must be due predominantly to oceanic tides. It is important to mention here that the conductivity of the ocean does not vary significantly with time, unlike the ionospheric conductivity. As a consequence, the seasonal variation of the oceanic contribution is expected to be smaller than the ionospheric contribution (Cueto et al., 2003).

In his review, Price (1969) suggested that the interpretation of field variations at a particular observatory must be done carefully. Although the ionosphere current system may have a fairly simple world-wide pattern, the relatively small variation of the conductivity distribution of the Earth's surface will introduce a corresponding small variation into the distribution of the induced currents.

3. Magnetic Data

In this section, we first describe the data used to study the quiet day variations. We also discuss the considerations used in data treatment for the different magnetic stations.

3.1. Dataset

In this paper, we used ground magnetic measurements to study the correlation between Vassouras (VSS - Brazil) and other 12 different magnetic stations, which we selected to provide a reasonably homogeneous distribution of measurements on the Earth's surface. The distribution of the magnetic stations, with their IAGA code, is given in Fig. 1. The corresponding codes and locations are given in Table 1. This work relied on data collections provided by the INTERMAGNET programme (<http://www.intermagnet.org>).

We chose the period of geomagnetically quiet days (through the Kp index, to evaluate magnetospheric disturbances) to study seasonal and solar activity variation. The data interval used

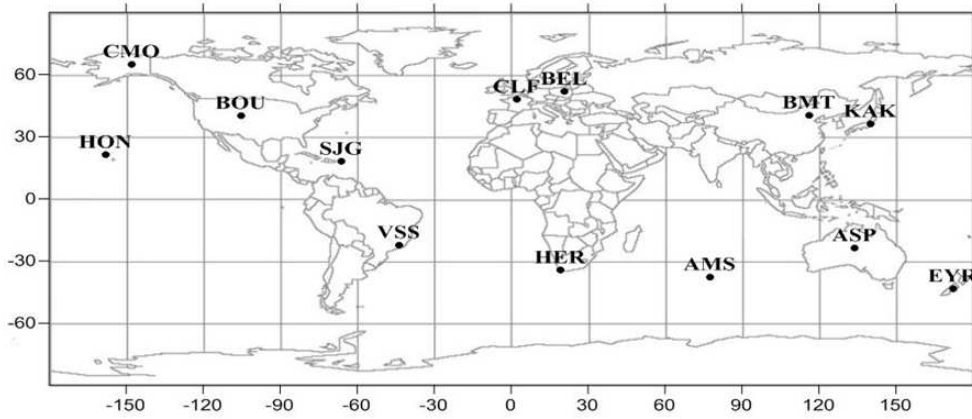


Figure 1: Geographical localization of the stations used in this work and their respective IAGA code.

in this work was from 1999 to 2007, almost the whole solar cycle 23 using the available dataset. In this data interval, the higher solar activity occurred between 2000 and 2001; and the lower solar activity, between 2005 and 2007. For seasonal variations, one year was divided into three seasons: June solstice, equinoxes (March and September) and December solstice.

To determine the disturbed days from the quiet days the Kp index was used. The global Kp index is a number from 0 to 9 obtained as the mean value of the disturbance levels within 3-h interval observed at 13 subauroral magnetic stations (see Bartels, 1957). Due to our interest in studying quiet days variations, we considered quiet days, only those days in which the sum of the Kp indices was less than or equal to 24 and the Kp index was not higher than 3. In our approach, the disturbed periods were eliminated and considered as gaps. Therefore, in principle only the magnetic effects of the lunar and solar contribution remained in the magnetic records.

3.2. Data Treatment Considerations

We used low- and mid-latitude magnetic stations so that the magnetograms for these days should be not seriously affected by auroral magnetic disturbances and the Sq would correspond to a regularly recurring phenomena in each day in these stations (Price, 1969).

In this work, we focus on the solar diurnal variations, and particularly, its diurnal and semidiurnal period spectral components. These features were greatly explored over the last decades, as well as their spatial dependence on latitude and others factors, including epoch of the year and level of solar activity (Price, 1969; Stening, 1971; Hibberd, 1985; Campbell, 1997; Le Sager and Huang, 2002; Takeda, 2002).

We took into consideration the two well known facts about the Sq field cited by Price (1969):

1. It is largely a local time field that can be roughly represented by a current fixed to the Sun, so we used the data at Universal Time (UT) to observe the global variance of the Sq field.
2. It is influenced by the Earth's main field throughout the latitudes between 60°N and 60°S , so we did not use magnetic stations of high latitudes (auroral zone).

Table 1: INTERMAGNET network of geomagnetic stations used in this study.

Station	Geografic coord.		Geomagnetic coord.	
	Lat.($^{\circ}$)	Long.($^{\circ}$)	Lat.($^{\circ}$)	Long.($^{\circ}$)
AMS	-37.83	77.56	-46.07	144.94
ASP	-23.76	133.88	-32.50	-151.45
BEL	51.83	20.80	50.05	105.18
BMT	40.30	116.20	30.22	-172.55
BOU	40.13	-105.23	48.05	-38.67
CLF	48.02	2.26	49.56	85.72
CMO	64.87	-147.86	65.36	-97.23
EYR	-43.42	172.35	-46.79	-106.06
HER	-34.41	19.23	-33.89	84.68
HON	21.32	-158.00	21.59	-89.70
KAK	36.23	140.18	27.46	-150.78
SJG	18.12	-66.15	27.93	6.53
VSS	-22.40	-43.65	-13.43	27.06

Source: <http://wdc.kugi.kyoto-u.ac.jp/igrf/gggm/index.html> (2010)

At high and polar latitudes, the geomagnetic field lines are aligned almost vertically so the ionospheric currents are joined with the field-aligned currents (FAC), and the electrodynamics is dominated by the influence of the solar-wind-magnetosphere interaction processes (Yomoto, 2006). On the other hand, the ionospheric current at middle and low latitude is generated by the influence of tidal winds, *i.e.*, ionospheric wind dynamo (Sastri, 1988).

Our primary interest was to correlate the response of the geomagnetic field at Vassouras to the other twelve previously chosen magnetic stations. The Vassouras Magnetic Observatory, is located in Rio de Janeiro, Brazil, under the South Atlantic Magnetic Anomaly (SAMA) influence. It has been active since 1915 and is a member of the INTERMAGNET programme. One of the peculiarities of VSS is its location, at a low latitude, where the H component is essentially the same as the total geomagnetic field. In forthcoming years, a Brazilian network of magnetometers will be implemented and VSS could be used as reference.

To fulfill our purpose, we used hourly mean value series of the H geomagnetic component. Some magnetic stations have available solely the X component, so we converted the X component of XYZ system to the H component of the HDZ system of vector representation of the Earths magnetic field (as described in Campbell, 1989). We used $X = H \cos(D)$, where X is the vertical component in the XYZ system, H is the horizontal magnitude and D is the angular direction of the horizontal component from the geographic north (declination). In principle, this system conversion does not affect our results because we only used magnetic stations of low- and mid-latitudes.

The magnetic stations that use the XYZ system are AMS, ASP, BEL and CLF. The conversion of systems was performed in BOU, CMO, EYR, HON and SJG for the data between 1999 and 2003 and in BMT and KAK for the data between 1999 and 2004.

An adequate knowledge of the daily variation field and a full understanding of the associated phenomena can only come from extensive and detailed analysis of the mean hourly values of the magnetic elements at many stations (Price, 1969). So the availability of these data in the World Data Centers that collect and distribute these data is of enormous help.

4. Methodology

The method used in this study is based on continuous wavelet transforms. In this section, we first introduce the concepts of the continuous wavelet transform (CWT) and its properties. Following, we introduce the gapped wavelet analysis and emphasize its improvements over the CWT. After that, we describe how we extracted the information of the observed data using wavelet cross-correlation analysis.

4.1. Continuous Wavelet Transform

The wavelet transform was introduced at the beginning of the 80s of the XX century by Morlet (1983), who used it to study seismic data. Grossmann and Morlet (1984) improved the windowed Fourier transform and they constructed the continuous wavelet transform (CWT). The idea was to change the width of the window function accordingly to the frequency of the signal being considered. The CWT is an integral transform, and it yields an affine invariant time-frequency representation. A wavelet transform can measure the time evolution of the frequency transients within the signal. In this transform, we use as basis, a set of functions called wavelets.

Formally, in order to be called wavelet, a function ψ must satisfy some conditions. First, the area under the curve described by the function ψ , must be zero,

$$\int \psi(t) dt = 0. \quad (1)$$

This condition is known as the admissibility condition and assures that the wavelet have a mean zero. Second, the function should be localized in both, physical and Fourier spaces (time and frequency), *i.e.*, the Heisenberg relation $\Delta t \Delta \omega = \text{const}$ must be satisfied.

The CWT of a time series f is defined by the integral transform,

$$W(a, b) = \int f(t) \psi_{a,b}^*(t) dt, \quad (2)$$

where $*$ represent the complex conjugate. This function $W(a, b)$ represents the wavelet coefficients that are function of both time and frequency (position b and scale a). It is obtained by dilating and translating the chosen analyzing wavelet and convolving it with the time serie ($f(t)$). The function ψ is expressed as

$$\psi_{a,b}(t) = \frac{1}{\sqrt{a}} \psi\left(\frac{t-b}{a}\right), \quad a > 0, a \in \mathbb{R}, \quad (3)$$

where the pre-factor $|a|^{-\frac{1}{2}}$ is introduced in order to guarantee that all the scaled functions $|a|^{-\frac{1}{2}} \psi(\frac{t}{a})$, have the same energy. The parameter b means a translation in time. However, the time-frequency resolution of the wavelet transform depends on scale a . We have good time localization (however, poor frequency localization) when a is small and vice-versa.

There are many possible analyzing wavelet. The choice of these wavelet depends on both: data and analysis objectives. Therefore, does not exist the best wavelet for signal analysis in general. For instance the Haar wavelet has a compact support in physical space and a large support in Fourier space, expected by the Heisenberg's uncertainty principle (as discussed in Daubechies, 1990). For relatively long data lenghts, smooth wavelet without a compact support (Maar and Morlet) can be used for computing CWT in terms of the Nyquist sampling theorem. The Maar wavelet is well localized in both, time and frequency, and it has a better localization in time than

185 the standart Morlet wavelet. Morlet wavelet is a complex wavelet and produces complex wavelet
 186 coefficients that gives us amplitude and phase information. In summary, the characteristic of the
 187 wavelet transform depends on the chosen analyzing wavelet. For instance, to study a time series
 188 with abrupt variations (steps) the Haar wavelet may be the most convenient; but for smoother
 189 time series Morlet and Maar wavelet are more recommended (see for instance Domingues et al.,
 190 2005, and references therein).

191 We used the Morlet wavelet,

$$\psi(t) = \exp\left(\frac{-t^2}{2\sigma^2}\right) \exp(i\omega_0 t), \quad (4)$$

192 with $i = \sqrt{-1}$, ω_0 is the frequency parameter and σ is the time resolution parameter. The
 193 adjustable parameter σ gives the optimal time-frequency resolution. Small values of σ give
 194 better time resolution, while large values improve frequency resolution. In the gapped wavelet
 195 case, the problem of the admissibility condition breaks down when σ is below 1. It must be
 196 avoided, and therefore, a wide range of σ should be used (as described in Soon et al., 1999).
 197 Here, after testing, we adopted $\omega_0 = 6$ and $\sigma = 1$ that also provides the better possible time-
 198 frequency equilibrium. In this case also, the Morlet wavelet is suited very well for experimental
 199 data analysis because it has a Gaussian envelope. It allows reach a reasonable compromise
 200 between the time-frequency resolutions.

201 It is possible to analyze a signal in a time-scale plane. In the wavelet analysis it is called
 202 the wavelet scalogram. In analogy with the Fourier analysis, the square modulus of the wavelet
 203 coefficient is used to provide the energy distribution in the time-scale plane. As in the Fourier
 204 analysis, we can also explore the dominant periods (or frequencies) of the time series through the
 205 global wavelet spectrum. It helps to understand the behaviour of the energy at a certain scale.

206 4.2. Gapped Wavelet Analysis

207 Magnetograms are finite length observational data series and may contain gaps of various
 208 sizes. To reduce gap problems, we use the gapped wavelet analysis a technique introduced by
 209 Frick et al. (1997) and afterwards improved in Frick et al. (1998). The mathematical properties
 210 of this algorithm were studied in detail. In this transform, the admissibility condition is broken
 211 when the wavelet overlaps data gaps. The leading idea of the gapped technique is to restore the
 212 admissibility condition by repairing in some way the wavelet itself.

213 Following Frick et al. (1997), we separate the analyzing wavelet in two parts, the oscillatory
 214 part $h(t)$ and the envelope $\varphi(t)$,

$$\psi(t) = h(t) \varphi(t), \quad (5)$$

$$h(t) = \exp(i\omega_0 t), \quad (6)$$

$$\varphi(t) = \exp\left(\frac{-t^2}{2}\right). \quad (7)$$

217 When the wavelet is disturbed by the gap, we can restore the admissibility condition by in-
 218 cluding a function $K(a, b)$ in the oscillatory part of the wavelet,

$$\widetilde{\psi}(t, b, a) = \left[h\left(\frac{t-b}{a}\right) - K(a, b) \right] \varphi\left(\frac{t-b}{a}\right) \quad (8)$$

219 and requiring,

$$\int \tilde{\psi}(t) dt = 0 \quad (9)$$

220 The introduced function $K(a, b)$ can be determined for each scale a and position b from (8)
221 and (9).

222 It was shown that this technique not only suppresses the noise caused by the gaps and bound-
223 aries, but improves the accuracy of frequency determination of short or strongly gapped signals
224 (Frick et al., 1998).

225 4.3. Wavelet Cross-correlation Analysis

226 The approach of this work is to use the wavelet cross-correlation to study the correla-
227 tion between a pair of magnetic data from different stations as a function of scale (see
228 Nesme-Ribes et al. (1995) and Frick et al. (2001) for more mathematical details):

$$C(a) = \frac{\int \mathcal{W}_1(a, t) \mathcal{W}_2^*(a, t) dt}{\left(\int \mathcal{W}_1(a, t)^2 dt \int \mathcal{W}_2(a, t)^2 dt \right)^{\frac{1}{2}}} \quad (10)$$

229 where $\mathcal{W}_i(a, t) = |W_i(a, t)| - \overline{|W_i(a, t)|}$, W_i are the wavelet coefficients and $\overline{W_i}$ is the arithmetic
230 mean in time for $i = 1$ or 2 . We can also obtain the determination coefficient as function of the
231 scale a . It is defined as the square of the correlation coefficient. One of the reasons to use the
232 coefficient of determination instead of the correlation is to compute the statistics to determine
233 the size or magnitude of the relation between two variables. It is interpreted as the percentage of
234 variance in one variable that is predicted or explained by the other. The correlation coefficient
235 permits the prediction of a score on one standardized variable from another, but this prediction
236 will be meaningful only if the relation between the two variables is approximately linear (see for
237 instance Ozer, 1985, and references therein). Though in space geophysics both the determination
238 and correlation coefficient are used. In our case, we preferred to use the determination coefficient
239 due to this interpretation of variance.

240 As we mentioned above, in the wavelet representation the scale (a) defines the distribution of
241 energy of the whole signal through time. The wavelet cross-correlation allows us to check the
242 interaction between two sets of data for each considered scale. The scales are chosen in such
243 a way that they make possible to characterize the dominating periods in the geomagnetic data
244 spectrum.

245 5. Results and Discussion

246 In order to exemplify the wavelet scalogram expected from the analysis of a daily magnetic
247 variation, we defined a synthetic Sq similarly to the described in Maslova et al. (2010),

$$S_q(t) = \sin\left(\frac{2\pi t}{24}\right) + \sin\left(\frac{4\pi t}{24}\right), \quad (11)$$

248 and the noise $R(t)$ as

$$R(t) = 0.5 * V(t) * \sin\left(\frac{2\pi t}{24}\right). \quad (12)$$

249 The good Sq estimative $Q(t)$ is given by

$$Q(t) = [S_q(t) + R(t)] * U(t), \quad (13)$$

250 where the day to day variability was introduced by the noise variables $V(t)$, $U(t)$ and $R(t)$, where
 251 $V(t)$ was uniformly distributed on $[0, 1]$ and $U(t)$ on $[0.5, 1.5]$.

252 Fig. 2(a), from top to bottom, shows the synthetic geomagnetic signal, the wavelet square
 253 modulus (scalogram) and phase with Morlet wavelet. It was possible to identify the two most
 254 prevailing periods (12 and 24-h) due to the quiet variations. Also, we can identify the change of
 255 frequencies introduced by the noise, which indicates that the wavelet analysis is useful for this
 256 multi-scale phenomena. The phase change was also analyzed, which allowed us to retrieve the
 257 oscillatory behavior of the data.

258 In Fig. 2(b), we used the same synthetic signal used in Fig. 2(a) with additional random gaps
 259 in the signal. The areas with gaps were signalized by arrows and dashed lines. We applied the
 260 gapped wavelet in this signal. In this new analysis, it was also possible to identify the quiet
 261 geomagnetic variations with periods of 12 and 24-h.

262 In an attempt to fill the gaps, we used cubic splines which led to an underestimation of high
 263 frequencies. As the signals may have many spectral components, only by using gapped wavelet,
 264 the high-frequency part of the spectrum can be reconstructed. For this reason, the gapped wavelet
 265 has some advantages over interpolation. However, the gapped wavelet has some limitations, it
 266 can only be used if the gap is not larger than the period of analysis.

267 After we performed the CWT and gapped wavelet in the synthetic signal, we concluded that
 268 the gapped wavelet fulfilled our purpose. Then, we started calculating the wavelet coefficients
 269 for each chosen station.

270 Fig. 3 shows an example of CWT applied to a real signal, in this case, a magnetogram data. In
 271 this analysis, we used the H component obtained in June, 2007 at VSS station. Fig. 3(a) shows
 272 the H component, (b) the wavelet square modulus (scalogram), (c) the global wavelet spectrum
 273 (total energy in each scale) and (d) the phase. Areas of stronger wavelet power are shown in
 274 dark red on a plot of time (horizontally) and time scale (vertically). In this wavelet power, it is
 275 not necessary to include the cone of influence because the gapped wavelet technique not only
 276 suppresses the boundary and gaps in both high and low frequencies, but also estimates better the
 277 frequency of the signal (see Frick et al. (1998) for mathematical proofs). Using gapped wavelet,
 278 we were able to determine both the dominant modes of variability and how these modes vary in
 279 time. In Fig. 3(b), the 24-h period shown in red is clearly visible and the 12-h period in the reddish
 280 color appears less dominantly compared to the 24-h. In Fig. 3(c), the global wavelet spectrum
 281 shows the pronounced increase of the total energy in the 24-h period and a less pronounced but
 282 still noticeable in the 12-h period.

283 The gapped wavelet used on the sythetic signal was then applied in real data as shown in
 284 Fig. 4. One might notice that Fig. 4 is very similar to Fig. 3, the difference is that now we
 285 introduced gaps due to disturbed days. As our interest was only to study the quiet day variations
 286 we considered the disturbed days (where the $Kp > 3$) as gaps. Even with the disturbed days, the
 287 global wavelet spectrum of Fig. 4 still shows a pronounced increase of energy in the 24-h and
 288 less dominant in the 12-h period. The inclusion of gaps in the data due to the removal of the
 289 disturbed days does not affect the analysis of the diurnal and semidiurnal variations. With the
 290 gapped wavelet coefficients in hand, we excluded the coefficients that corresponded to the gaps
 291 areas in the scalograms. The excluded areas are presented as white rectangles in Fig. 4.

292 After the gapped wavelet analysis, we have calculated the cross-correlation functions $C(a)$, for

each pair formed by Vassouras and one of the twelve chosen magnetic stations. This procedure was done for the years 1999 to 2007 during the equinoxes and solstices. These calculations were performed in order to understand the global response of the Sq variation at different locations.

Fig. 5 shows the modulus of the correlations functions (for June, 2007) for the twelve magnetic stations. The correlation graphics are displayed from top to bottom and divided in two blocks, in the same order as in Table 1. These selected stations are divided in low latitude (ASP, BMT, HER, HON, KAK and SJG), medium latitude (AMS, BEL, BOU, CLF and EYR) and high latitude (CMO). In the vertical axis, we present the correlation coefficients and in the horizontal axis, the scale (period in hours). The periods of 24, 12, 8 and 6-h are highlighted with dashed lines in order to facilitate visual inspection and comparison (see Fig. 5). It was possible to verify that for most of the pairs $C(a)$ varies considerably with scale. We observed that the correlation between two geomagnetic data sets is scale dependent. They were strongly correlated or less correlated depending on the scale. We also observed that the correlation was usually larger for the first harmonics of the diurnal variations, and consequently got smaller and smaller for the following harmonics. Through Fig. 5, we determined the correlation for 24 and 12-h periods and also calculated the determination coefficients.

As mentioned before, the principal driven forces of the Sq currents are due to the daily thermal-tidal motions and the thermospheric winds moving the ionization through the Earth's magnetic field. During the solstices, there is a wind asymmetry between the Northern and Southern hemispheres due to the contrast in summer-winter radiation. In Fig. 5, we expected a small correlation between VSS and the magnetic stations located in the Northern hemisphere (BEL, BMT, BOU, CMO, HON, KAK and SJG) as a result of the month of June be a solstice: the thermosphere wind asymmetry during the minimum solar activity is not as larger as during the maximum solar activity. Also in Fig. 5, some stations located in the Northern hemisphere presented a larger correlation with VSS what can be attributable to the latitudinal dependence of the Sq current. Magnetic stations located at lower latitudes as VSS presented larger correlation (HON and SJG).

Fig. 6 and 7 present the graphics of the diurnal and semidiurnal geomagnetic variations, respectively. These figures show the determination coefficient for the 12 chosen stations during the equinoxes and solstices between the years of 1999 and 2007. In the vertical axis, we present the determination coefficient and in the horizontal axis, the twelve chosen magnetic stations ordained in latitude from the southern to the northern hemisphere. This distribuion of stations helped to verify the latitudinal dependence of the diurnal variations. To validate their seasonal behaviour, we obtained the determination coefficient on March, June, September and December. In Fig. 6 and 7, March is displayed at top left, June at top right, September at bottom left and December at bottom right. We performed this analysis for the interval from high (1999) to low (2007) solar activity. This interval enabled the study of the solar activity dependence upon the Sq variations. Years of high solar activity are shown in black (corresponding to the mean value of the determination coefficient for the years of 1999, 2000 and 2001), years of medium solar activity, in grey (corresponding to the mean value of the determination coefficient for the years of 2002, 2003 and 2004) and years of low solar activity, in white (corresponding to the mean value of the determination coefficient for the years of 2005, 2006 and 2007).

In Fig. 6, it was possible to identify a primary latitudinal dependence for the equinoxes and solstices. If we consider the simple dipole representation of the Earth's main magnetic field and the north-south symmetry of thermospheric wind and conductivity field between hemispheres in equinox conditions, we would find that the stations at the same latitude should have the same determination coefficient. However, the geomagnetic field is asymmetric so the mean conductance for the northern and southern hemisphere will have different values even at equinox (Stening,

1971). This characteristic may explain the difference of response between some magnetic stations located at similar magnetic latitudes but at different hemispheres.

The disparity in the response of magnetic station between solstices is expected. These differences between the determination coefficients could be explained by the following features of the Sq field reported by Matsushita and Maeda (1965): 1) the total Sq current intensity is about 1.5 times larger in the hemisphere's summer than in the winter and 2) the latitudinal position of the external current center is higher in summer than in winter.

In this work, we also found that the 24-h diurnal variation presented differences in the determination coefficient for magnetic stations located in approximately the same geomagnetic latitude but different longitudes. This mean that these stations were affected differently by the E-layer dynamo. At equinoxes, the determination coefficient was usually larger in years of higher solar activity, and at solstices it was practically larger in the year of lower solar activity. These results may be explained by the variation of conductivity of the E-region which has a ionization density dependency (Forbes and Lindzen, 1976). Also, the total geomagnetic field affects the conductivity through it dependence on electron and ions gyro-frequencies (Stening, 1971).

Another strong influence, very important to refer, is the intensity of the geomagnetic field. The total geomagnetic field is particularly high in the regions of central Canada, Siberia and south of Australia and it is quite low near southern Brazil (Campbell, 1997). In Fig. 6, it was possible to observe that the magnetic stations, located at the northwest of Canada (CMO), north of the United States (BOU), China (BMT), Japan (KAK) and the central of Australia (ASP), where the geomagnetic field is particularly high, presented lower determination coefficient when compared to other stations.

For the semi-diurnal variation, the latitudinal dependence was not as perceptible as in the diurnal variation (see Fig. 6 and 7). Also, the equinoxes and solstices presented irregular distribution due to the solar activity.

We expected lower correlation between VSS and CMO, because CMO is the station located at the highest latitude. The influence of the Sq currents is limited at high latitudes when compared to low and mid-latitudes. At high latitudes, the major influence comes from a large horizontal current that flows in the D and E regions of the auroral ionosphere, called the Auroral Electrojet. There are two characteristic of the auroral region that we must mention. First of all, the conductivity in the auroral ionosphere is generally larger than at lower latitudes. Second, the horizontal electric field in the auroral ionosphere is also larger than at lower latitudes. Since the strength of the current flow is directly proportional to the vector product of the conductivity and the horizontal electric field, the auroral electrojet currents are generally larger if compared to those at lower latitudes (see Sizova (2002) for more details).

Magnetic stations and observatories on islands or coastlines are fully exposed to anomalous effects of the ocean (Schmucker, 1999a,b). The oceans, as well as the ionosphere, constitute electrical conductors and they are subject to tidal motions. As a result of the tidal flow of the ocean water, we might expect the effects of some kind of dynamo (Parkinson, 1983). The electric current system induced by the oceanic tides due to the drifting motion produces some kind of daily variation on magnetic stations located at oceanic islands and nearby shores. This shows that caution must be taken when interpreting the solar magnetic variations at a particular station, if the purpose is to obtain a world-wide analysis of the Sq field.

The total variation measured on the ground consists of both external (ionospheric current) and internal (induced Earth current) contributions (Forbes and Lindzen, 1976). The pattern of the conductivity of surfaces layers of the Earth will introduce a corresponding small scale pattern into the distribution of the induced currents. At certain stations, an accurate indication of the

average induced current system is difficult to determine, consequently its effects can not be fully distinguished (Price, 1969). However, the intensity of the external origin of the Sq field is about 2.5 times that of the internal origin (Matsushita and Maeda, 1965). Therefore, in this work, we disregarded the influence of the internal contributions on the analysis of the diurnal geomagnetic variations.

6. Conclusions

A world-wide distribution of the harmonic components of solar diurnal variations (24 and 12-h periods) has been observed in latitude and longitude by using the gapped wavelet analysis and the wavelet cross-correlation technique. The objective of this paper was to study the characteristics of these variations at a Brazilian station as compared to the features from other magnetic stations to better understand the dynamics of the diurnal variations involved in the monitoring of the Earth's magnetic field. The main results in this analysis can be summarized as follows:

1. The difference in the mean conductance due to the asymmetry of the geomagnetic field might be responsible for the difference in the latitudinal response between the magnetic stations, even at the equinoxes.
2. We observed lower determination coefficients in the magnetic stations located on areas of the terrestrial globe where the geomagnetic field is particularly high.
3. For the diurnal variation, the determination coefficient was usually larger in years of higher solar activity at the equinoxes and practically smaller in years of lower solar activity at solstices.
4. The dependency of the E-region conductivity on the ionization density might explain the variation of the determination coefficient due to the solar activity.
5. The variation of the E-region conductivity according to the intensity of the geomagnetic field might account for the differences of the determination coefficient among different stations.
6. The latitudinal dependence for the semi-diurnal variation was not as noticeable as for the diurnal variation, and also, it presented an irregular distribution due to the solar activity.
7. In closing, this analysis showed that there were unusual and unequal contributions for each station according to their correlation to VSS.
8. The analysis performed has shown a great spatial and temporal variability of the diurnal variation. These results suggest that the quiet days patterns and the physical processes involved still remain an important issue, that is far from being fully understood.

The gapped wavelet analysis is an alternative technique to study data series that contain gaps of various sizes. Consequently, it can be used to exclude disturbed days and to study the characteristics of solar diurnal variations. Using a network of magnetic stations, we determined the contributions of the longitude and latitude and also of the total geomagnetic field.

7. Acknowledgments

V. Klausner wishes to thanks CAPES for the financial support of her PhD. A. R. R. P. thanks CNPq for a research fellowship. This work was supported by CNPq (grants 309017/2007-6, 486165/2006-0, 308680/2007-3, 478707/2003, 477819/2003-6, 382465/01-6), FAPESP (grants 2007/07723-7) and CAPES (grants 86/2010-29). We are grateful to V. E. Menconni (FAPESP 2008/09736-1) for their helpful computational assistance. Also, the authors would like to thank the INTERMAGNET programme for the datasets used in this work.

References

- Bartels, J., 1957. The technique of scaling indices k and q of geomagnetic activity. *Annals of the International Geophysical Year* (4), 215–226.
- Campbell, W. H., 1989. An introduction to quiet daily geomagnetic fields. *Pure and Applied Geophysics* 131 (3), 315–331.
- Campbell, W. H., 1997. *Introduction to Geomagnetic Fields*. Cambridge University Press, New York.
- Chapman, S., Bartels, J., 1940. *Geomagnetism*. Oxford University Press, London.
- Chapman, S., Stagg, J. M., 1929. On the variability of the quiet day diurnal magnetic variation at eskdalemuir and greenwich. *Proceedings of the Royal Society London A* 123, 27–53.
- Cueto, M., McKnight, D., Herraiz, M., 2003. Daily geomagnetic variations on the iberian peninsula. *Geophysical Journal International* 152 (1), 113–123.
- Daubechies, I., Sep. 1990. The wavelet transform, time-frequency localization and signal analysis. *IEEE Transactions on Information Theory* 36 (5), 961–1005.
- Domingues, M. O., Mendes, O. J., Mendes da Costa, A., 2005. Wavelet techniques in atmospheric sciences. *Advances in Space Research* 35 (5), 831–842.
- Forbes, J., Lindzen, R. S., 1976. Atmospheric solar tides and electrodynamics effects. i. the global sq current system. *Journal of Atmospheric and Solar-Terrestrial Physics* 38, 897–910.
- Frick, P., Baliunas, S. L., Galyagin, D., Sokoloff, D., Soon, W., 1997. Wavelet analysis of stellar chromospheric activity variations. *The Astrophysical Journal* 483 (1), 426–434.
- Frick, P., Beck, R., Berkhuijsen, E. M., Patrickeyev, I., 2001. Scaling and correlation analysis of galactic images. *Monthly Notices of the Royal Astronomical Society* 327 (4), 1145–1157.
- Frick, P., Grossmann, A., Tchamitchian, P., 1998. Wavelet analysis of signal with gaps. *Journal of Mathematical Physics* 39 (8), 4091–4107.
- Graham, G., Watchmaker, F. R. S., 1724. An account of observations made of the variation of the horizontal needle at london, in the latter part of the year 1722, and beginning of 1723. *Philosophical Transactions* 33, 96–107.
- Grossmann, A., Morlet, J., 1984. Decomposition of hardy functions into square integrable wavelets of constant shape. *SIAM Journal on Mathematical Analysis* 15 (4), 723–736.
- Hibberd, F. H., 1985. The geomagnetic sq variation - annual, semi-annual and solar cycle variations and ring current effects. *Journal of Atmospheric and Solar-Terrestrial Physics* 47, 341–352.
- Larsen, J., Cox, C., 1966. Lunar and solar daily variation in the magnetotelluric field beneath the ocean. *Journal of Geophysical Research* 71, 4441.
- Le Sager, P., Huang, T. S., 2002. Ionospheric currents and field-aligned currents generated by dynamo action in an asymmetric earth magnetic field. *Journal of Geophysical Research* 107 (A2), 1025.
- Maslova, I., Kokoszka, J., Sojka, L., Zhu, L., 2010. Estimation of sq variation by means of multiresolution and principal component analyses. *Journal of Atmospheric and Solar-Terrestrial Physics* 72, 625–632.
- Matsushita, S., Maeda, H., 1965. On the geomagnetic solar quiet daily variation field during the igy. *Journal of Geophysical Research* 70 (11), 2535–2558.
- Morlet, J., 1983. Sampling theory and wave propagation. In: Chen, C. (Ed.), *Acoustic Signal/Image Processing and Recognition*, in NATO ASI. Springer-Verlag, New York., Vol. 1. pp. 233–261.
- Nesme-Ribes, E., Frick, P., Sokoloff, D., Zakharov, V., Ribes, J. C., Vigouroux, A., Laclare, F., 1995. Wavelet analysis of the maunder minimum as recorded in solar diameter data. *Comptes rendus de l’Académie des sciences. Série II, Mécanique, physique, chimie, astronomie* 321 (12), 525–532.
- Oczereko, E., Swiatecka, J., Kitlas, A., Laudanski, T., Pierzynski, P., 2006. Visualization of synchronization of the uterine contraction signals: running cross-correlation and wavelet running cross-correlation methods. *Medical engineering & physics* 28 (1), 75–81.
- Ozer, D. J., 1985. Correlation and the coefficient of determination. *Psychological Bulletin* 97 (2), 307–315.

476 Parkinson, W. D., 1983. Introduction to geomagnetism. Scottish Academy Press, Edinburg and London.

477 Price, A. T., 1969. Daily variations of the geomagnetic field. *Space Science Reviews* 9 (2), 151–197.

478 Rehman, S., Siddiqi, A. H., 2009. Wavelet based correlation coefficient of time series of saudi metereological data.

479 *Chaos, Solitons & Fractals* 39 (4), 1764–1789.

480 Sastri, J. H., 1988. Equatorial electric fields of ionospheric disturbance dynamo origin. *Annales Geophysicae* 6 (6),

481 635–642.

482 Schmucker, U., 1999a. A spherical harmonic analysis of solar daily variations in the years 1964–1965: response esti-

483 mates and source fields for global inductioni. methods. *Issue Geophysical Journal International Geophysical Journal*

484 *International* 136 (2), 439–454.

485 Schmucker, U., 1999b. A spherical harmonic analysis of solar daily variations in the years 1964–1965: response estimates

486 and source fields for global inductionii. results. *Geophysical Journal International* 136 (2), 455–476.

487 Sizova, L. Z., 2002. The field-aligned currents effect on equatorial geomagnetic field variations. *Advances in Space*

488 *Research* 30, 2247–2252.

489 Soon, W., Frick, P., Baliunas, S., 1999. Lifetime of surface features and stellar rotation: a wavelet time-frequency

490 approach. *The Astrophysical Journal* 510 (2), 135–138.

491 Stening, R. J., 1971. Longitude and seasonal variations of the sq current system. *Radio Science* 6 (2), 133–137.

492 Stewart, B., 1882. Terrestrial magnetism. Vol. 16 of *Encyclopaedia Britannica*. Encyclopaedia Britannica Inc., London.

493 Takeda, M., 1999. Time variation of global geomagnetic sq field in 1964 and 1980. *Journal of Atmospheric and Solar-*

494 *Terrestrial Physics* 61 (10), 765–774.

495 Takeda, M., 2002. The correlation between the variation in ionospheric conductivity and that of the geomagnetic sq field.

496 *Journal of Atmospheric and Solar-Terrestrial Physics* 64 (15), 1617–1621.

497 Yomoto, K., 2006. The MAGDAS Group, in *Solar Influence on the Heliosphere and Earths Environment: Recent*

498 *Progress and Prospects*. N. Gopalswamy and A. Bhattacharyya, Goa, India.

499 Zhao, B., Wan, W., Tschu, K., Igarashi, K., Kikuchi, T., Nozaki, K., Watari, S., Li, G., Paxton, L. J., Liu, L., Ning,

500 B., Liu, J.-Y., Su, S.-Y., Bulanon, H. P., 2008. Ionosphere disturbances observed throughout south- east asia of the

501 superstorm of 20 – 22 november 2003. *Journal of Geophysical Research* 113 (A00A04).

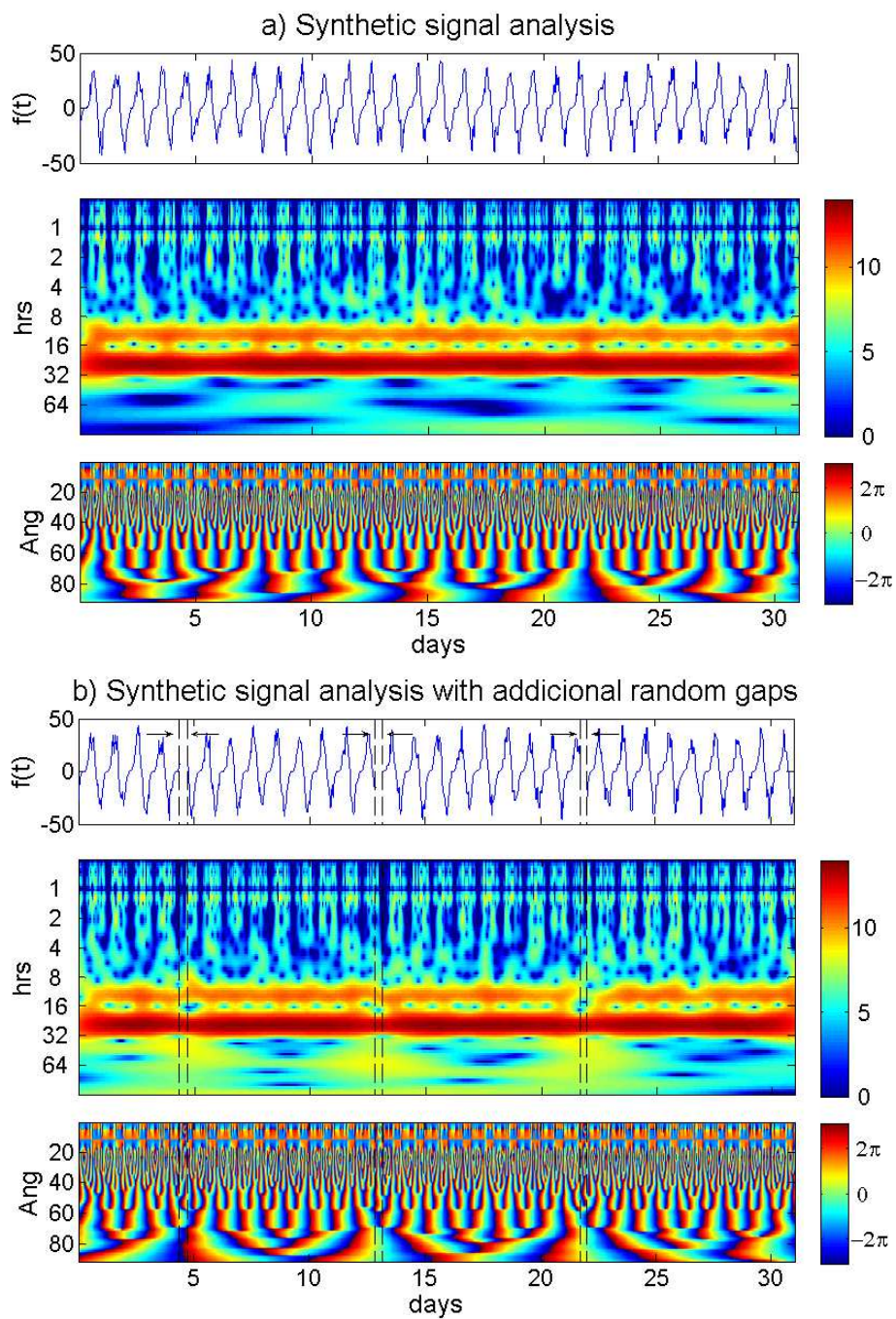


Figure 2: Two spectrograms of synthetic signal consisting of a daily magnetic variation: (a) the synthetic signal and (b) the synthetic signal with additional random gaps. From top to bottom, each spectrogram shows: the synthetic signal (signal with gaps), the continuous wavelet (gapped wavelet) spectrogram which satisfactorily resolves both in time and frequency and the phase change of the data.

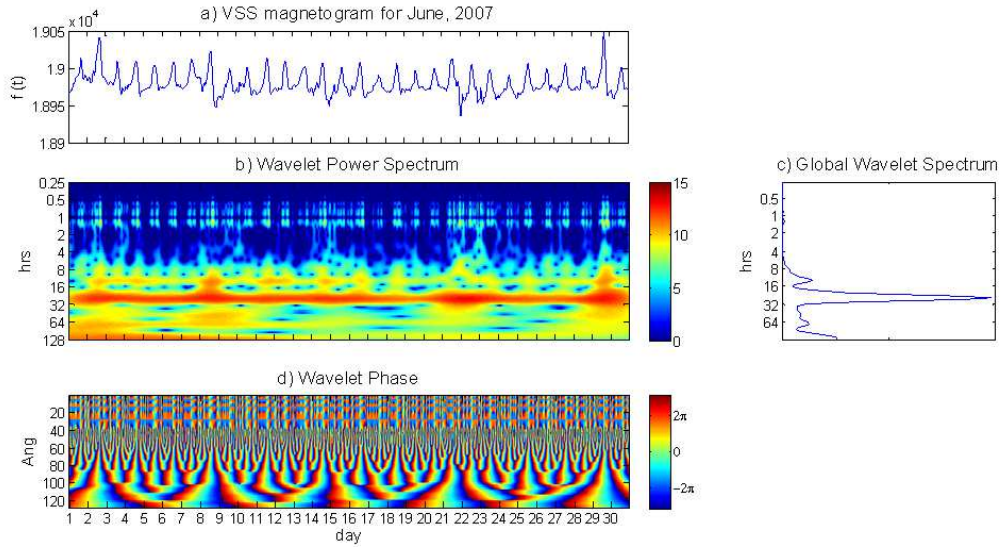


Figure 3: Each panel shows: (a) H component time series of VSS Station at June, 2007 used for the wavelet analysis, (b) the local wavelet power spectrum using Morlet wavelet, logarithmic scaled, (c) the global wavelet spectrum and (d) the phase spectrum.

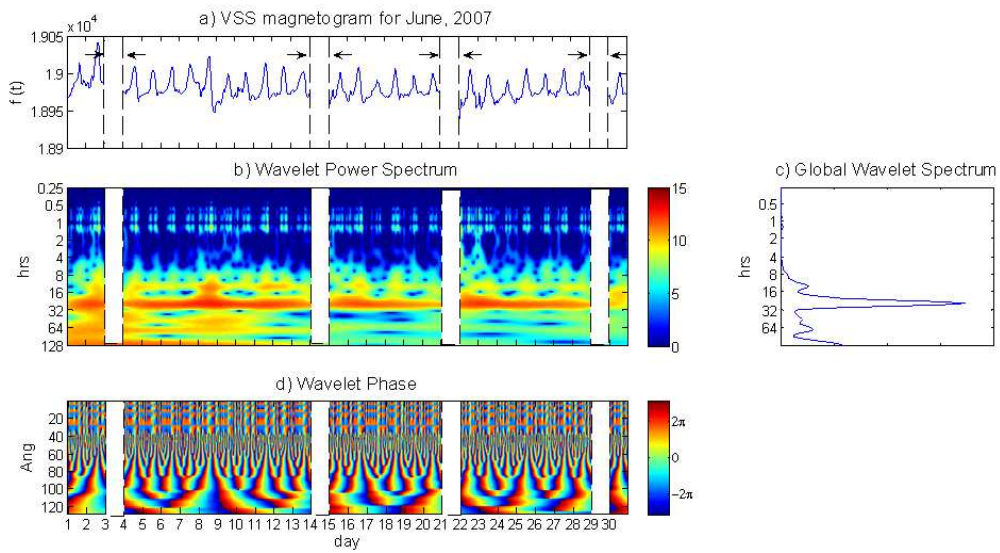


Figure 4: Each panel shows: (a) H component time series of VSS Station at June, 2007 with additional gaps due to the disturbed days; (b) the local wavelet power spectrum using Morlet wavelet, logarithmic scaled, (c) the global wavelet spectrum and (d) the phase spectrum.

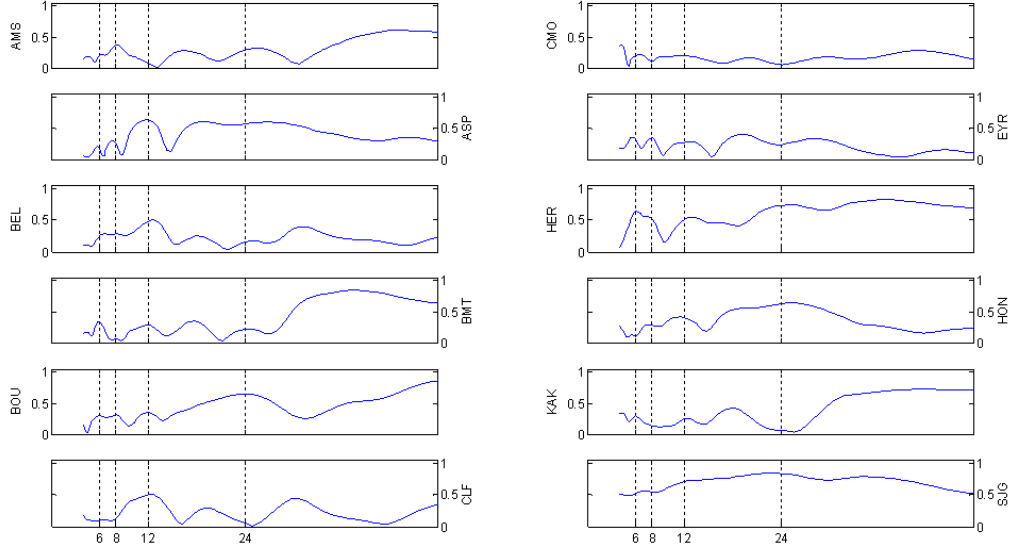


Figure 5: Modulus of the wavelet cross-correlation functions for each pair formed by VSS and one of the twelve chosen magnetic stations for June, 2007.

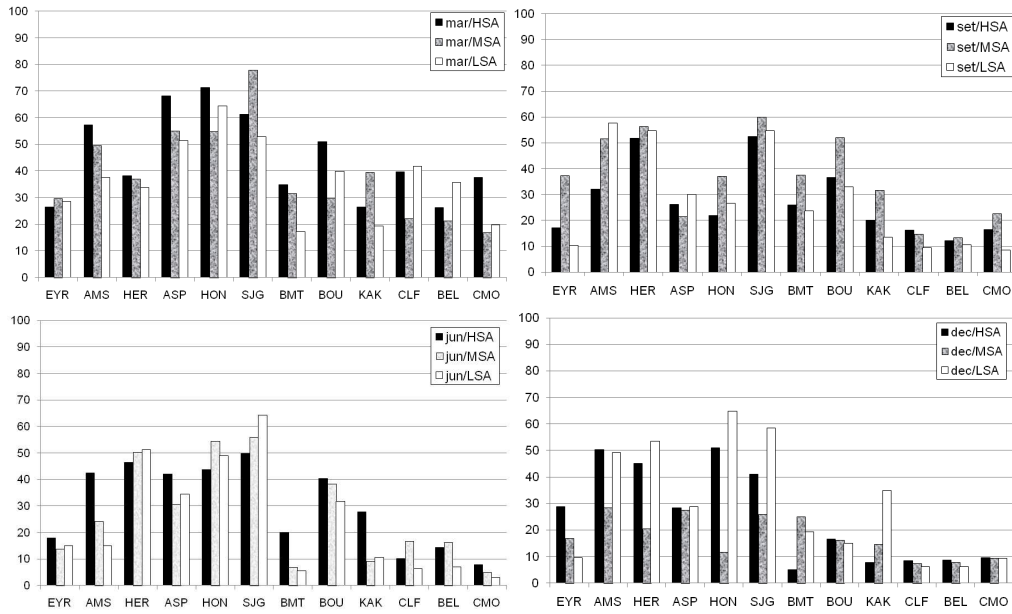


Figure 6: Graphs of the diurnal geomagnetic variation during the equinoxes (March and September) and solstices (June and December) months, and the years from 1999 (high solar activity) to 2007 (low solar activity). The vertical axis shows the mean of determination coefficient and the horizontal shows the ABB code of the stations distributed by latitude.

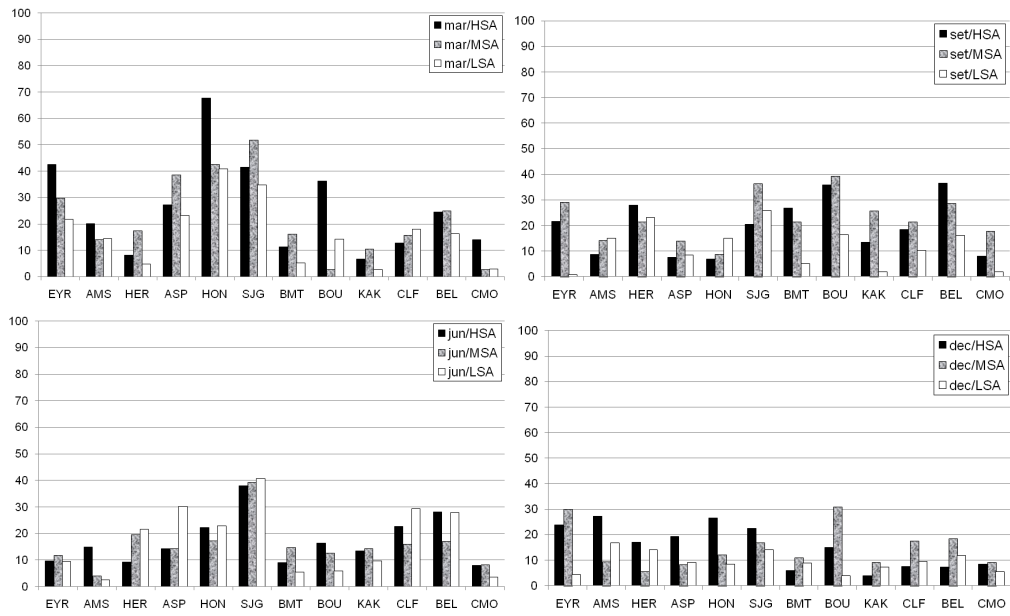


Figure 7: Graphs of the semidiurnal geomagnetic variation during the equinoxes (March and September) and solstices (June and December) months, and the years from 1999 (high solar activity) to 2007 (low solar activity). The vertical axis shows the mean of determination coefficient and the horizontal shows the ABB code of the stations distributed by latitude.